Magnetized implosions driven by intense ion beams

M. M. Basko[a)]
Gesellschaft für Schwerionenforschung, Planckstr. 1, D-64291 Darmstadt, Germany

(Received 2 May 2000; accepted 2 August 2000)

Intense beams of heavy ions, envisaged for the near future at the Institute for Theoretical and Experimental Physics (Moscow) and Gesellschaft für Schwerionenforschung (Darmstadt), will be well suited for conducting implosion experiments in cylindrical geometry. In such implosions, the initial pressure generated by the direct beam heating can be enhanced by more than a factor of 10. If, in addition, an external magnetic field is introduced, the effect of magnetothermal insulation may allow to reach kilovolt temperatures and significant thermonuclear neutron yields in magnetized implosions driven by the beam heating intensities as low as $\dot{\epsilon}\simeq 1$ TW/g. It is shown how the combined effect of the electrical resistivity and thermal conductivity sets a lower limit on the product UR (R is the radius, and U is the velocity of an imploding plasma volume) as a necessary condition for the regime of self-sustained magnetized implosion (SSMI). The optimal plasma parameters required for initiation of this regime are evaluated. In cylindrical geometry, the threshold for the SSMI regime is determined by the total driver energy deposition per unit areal density of the cylinder, $\rho^{-1}|dE_b/dz|$ (kJ cm^2/g). The results of one-dimensional magnetohydrodynamic simulations indicate that the advantages of magnetized implosions begin to manifest themselves at a beam energy level of $E_b\approx 100$ kJ. © *2000 American Institute of Physics.*
[S1070-664X(00)01911-X]

I. INTRODUCTION

Once intense beams of heavy ions become available,[1–3] they will offer a new way of generating high energy density states in matter. On the one hand, experiments with ion-beam generated plasmas can be considered as a first step toward controlled fusion driven by heavy ion beams. On the other hand, due to special features of the energy deposition mechanism by fast ions, such experiments can make a contribution of their own to fundamental plasma physics research.

In the simplest case, a quasicylindrical plasma volume can be created by focusing an ion beam onto a uniform sample. The peak pressure and temperature values that can be attained in this way and the ensuing hydrodynamic motion have been analyzed recently by Tahir *et al.*[4,5] for realistic beam parameters of the heavy ion synchrotron at the Gesellschaft für Schwerionenforschung (GSI) in Darmstadt (Germany). In such simple experiments, if one aims at matter states with maximum concentration of energy, hydrodynamic expansion plays a negative role by weakening the pressure and temperature peaks in irradiated targets. At the same time, hydrodynamic flow in a converging geometry can be employed to enhance the initial energy concentration created by the beam heating. In this paper we examine the possibility of using cylindrical implosions in combination with the effect of magnetic insulation to achieve maximum possible pressures and temperatures in the compressed plasma column along the target axis.

The cylindrical symmetry of hydrodynamic motion arises naturally in experiments with energetic ions ($E_i/A_i \gtrsim 0.5-1$ GeV/u) envisaged for the future facilities at the Institute for Theoretical and Experimental Physics (ITEP) in Moscow (Russia)[1] and at the GSI.[2,3] Such ions can be focused on a circular spot of a submillimeter diameter and have a multimillimeter range even in the most dense materials, thus creating a long cylindrical channel of heated matter in a target. As specific examples, we quote the parameters of the TeraWatt Accumulator (TWAC) beam at ITEP,[1] $N_i=1.2\times 10^{13}$ ions of $_{59}\mathrm{Co}^{+27}$ with the kinetic energy of $E_i/A_i=0.7$ GeV/u and the total beam energy of $E_b\equiv N_iE_i\approx 100$ kJ, and those of the High-current Accumulator Ring (HAR) proposed for the future GSI synchrotron,[3] $N_i=10^{12}$ ions of $_{131}\mathrm{Xe}^{+54}$ with the kinetic energy of $E_i/A_i=1.1$ GeV/u and the total beam energy of $E_b\approx 20$ kJ. Within 10% accuracy, these two beams have equal stopping ranges of $\langle\rho l\rangle_i\approx 30$ g/cm^2 in solid gold, and $\langle\rho l\rangle_i\approx 15$ g/cm^2 in gaseous (1 atm) deuterium. When we take the corresponding values of the focal spot radius, $r_{\mathrm{foc}}=0.8-1.0$ mm for the TWAC beam[1] and $r_{\mathrm{foc}}=0.4$ mm for the HAR beam,[3] we calculate essentially the same value of the specific energy deposition,

$$\epsilon=\frac{1}{\pi r_{\mathrm{foc}}^2}\frac{N_i}{\rho}\left|\frac{dE_i}{dz}\right|_{z=0}\approx\begin{cases}100\ \text{kJ/g in gold},\\ 200\ \text{kJ/g in deuterium},\end{cases}\qquad(1)$$

for both cases. Here $E_i=E_i(z)$ is the energy of individual ions as a function of the coordinate z along the beam trajectory. Hydrodynamic consistency between the above values of ϵ and r_{foc} sets a limit on the ion pulse duration $t_p\lesssim(100\ \text{ns})(r_{\mathrm{foc}}/1\ \text{mm})$, which agrees reasonably well with the capabilities of the ion bunch compression technique.[1–3]

[a)]On leave from the Institute for Theoretical and Experimental Physics, Moscow, Russian Federation; electronic mail: basko@vitep5.itep.ru

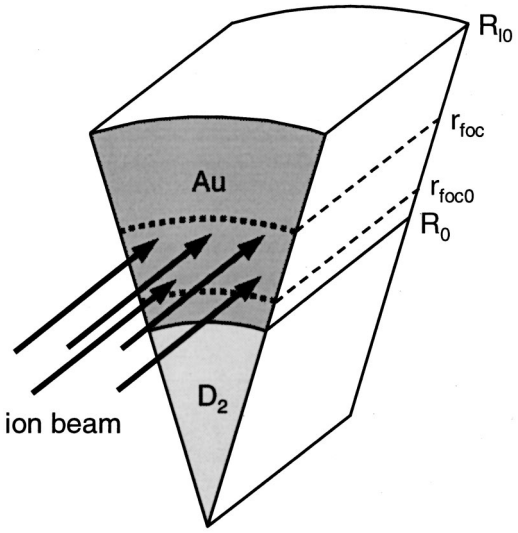

FIG. 1. Schematic view of a cylindrical target for implosion experiments with ion beams. The implosion is driven by an annular beam irradiating a gold liner layer at $r_{\mathrm{foc}0}<r<r_{\mathrm{foc}}$.

The specific driver energy deposition (1) is used as a reference value in all the hydrodynamic and magnetohydrodynamic (MHD) simulations discussed below.

Magnetized cylindrical implosions of hydrogen-isotope plasma columns have been discussed previously in the context of ultrahigh magnetic field generation in gas-puff Z pinches,[6,7] and with imploded metallic liners.[8] The quality of the magnetic field confinement was characterized by controlling the corresponding magnetic Reynolds values Rm. However, to the author's knowledge, the parametric analysis of magnetized implosions has never been carried out in such a way as to single out the regime of self-sustained magnetized implosion (SSMI) and to derive the necessary condition (17) for reaching this regime. This latter condition originates from simultaneous constraints on the magnetic Reynolds and the Péclet numbers of a magnetized plasma volume compressed by a liner. The SSMI regime is, of course, of critical importance for the concept of magnetized target fusion (MTF), although its comprehensive parametric analysis is missing in the published work on MTF (see Ref. 9 and references therein). The SSMI conditions derived in this paper should provide a useful guidance when one is exploring the large parameter space of the MTF targets.

II. PRESSURE PEAK ENHANCEMENT IN CYLINDRICAL IMPLOSIONS

The imploding configuration that we consider here is shown in Fig. 1. It consists of a metallic tube (liner) filled with a low-density deuterium gas, which is referred to as thermonuclear fuel. The initial inner and outer liner radii are, respectively, R_0 and R_{l0}. We assume that fast ions propagate along the cylinder axis and heat matter uniformly inside the focal radius r_{foc} during the pulse of duration t_p at a constant rate,

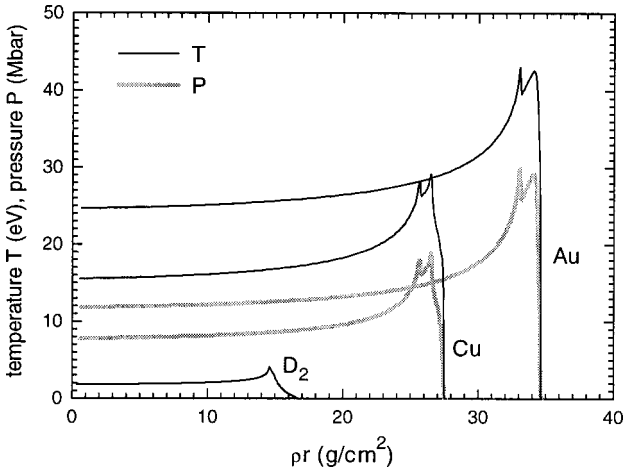

FIG. 2. Pressure and temperature profiles along the trajectory of 1.1 GeV/u Xe ions in three different target materials after a short pulse with the irradiation intensity of 2×10^{14} ions/cm^2.

$$\dot{\epsilon}=\begin{cases} 1.0\left(\dfrac{100\ \mathrm{ns}}{t_p}\right) & \mathrm{TW/g\ \ in\ \ gold,} \\ 2.0\left(\dfrac{100\ \mathrm{ns}}{t_p}\right) & \mathrm{TW/g\ \ in\ \ deuterium,} \end{cases} \tag{2}$$

which corresponds to the total energy deposition of $\epsilon=100$ kJ/g in gold.

To check the uniformity of the ion energy deposition along the cylinder length under realistic experimental conditions, a separate one-dimensional (1-D) run has been performed for stopping of the 1.1 GeV/u Xe ions in the plane-parallel geometry. The ion fluence was fixed at a value of $N_i/(\pi r_{\mathrm{foc}}^2)$ for $N_i=10^{12}$ and $r_{\mathrm{foc}}=0.4$ mm. The pulse duration was set artificially short, $t_p=0.1$ ns, in order to avoid complications due to the hydrodynamic expansion. The resulting temperature and pressure profiles along the ion trajectory at the end of the ion pulse $t=t_p$ are shown in Fig. 2 for three different target materials. For gold and copper, normal initial densities were assumed, deuterium was simulated at $\rho_0=10^{-3}$ g/cm^3. Figure 2 demonstrates that the ion energy deposition is uniform to within 10% along the initial 60%–70% of the range, which corresponds to a $\gtrsim$1 cm long cylinder of gold, and to an almost 2 cm long cylinder of copper. The double-hump structure of the Bragg peak in gold and copper is caused by the specific temperature dependence of the ion stopping power in dense plasmas inherent in the stopping model used for the present calculations and discussed in detail in Ref. 10. From this figure one learns also that the highest pressure in static matter is achieved in high-Z materials with the highest initial density. This explains why gold was chosen as the target material for simulations discussed below.

In this work we distinguish between two different cases of target irradiation, which correspond to two different implosion patterns. The simplest configuration, referred to as the case of exploding pusher, is realized with a uniform beam profile, when the ion current fills the entire beam cross section at $0<r<r_{\mathrm{foc}}$. The gaseous cavity is then imploded by the hot metallic vapor of the unloading inner edge of the

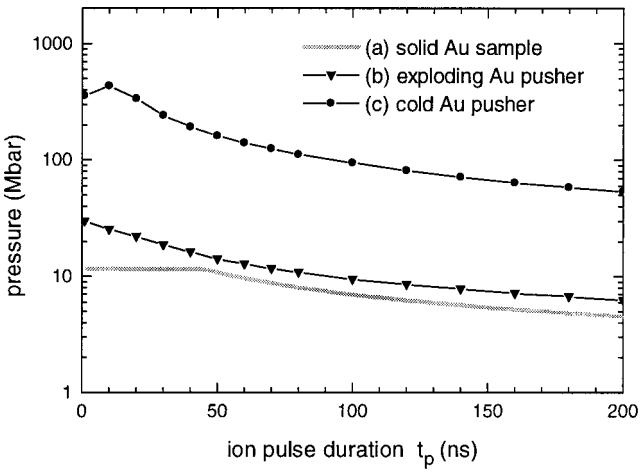

FIG. 3. Peak pressure values on the target axis versus ion pulse duration t_p. The beam specific energy deposition and its focal radius are fixed, respectively, at $\epsilon=100$ kJ/g and $r_{foc}=0.4$ mm. Two implosion configurations (b) and (c) (see the text) are compared with the simplest case (a) of solid sample irradiation.

heated liner. The second case of cold pusher requires a hollow (annular) ion beam, which heats the liner material only in the annular region $r_{foc0}<r<r_{foc}$. Again, we assume that the heating rate in this region is given by Eq. (2). In this case the cavity is imploded by the cold inner portion of the liner originally at $R_0<r<r_{foc0}$, which is accelerated inward by heated matter at $r_{foc0}<r<r_{foc}$. Note that, while the inner, $R(t)$, and the outer, $R_l(t)$, edges of the liner move, the boundaries of the energy deposition region, r_{foc0} and r_{foc}, remain fixed. There may be different methods of creating hollow beams by either an appropriate target design or beam manipulations, but we do not discuss them in this paper.

Figure 3 shows the peak pressure values attained on the cylinder axis in 1-D hydrodynamic simulations when the imploding liner is halted by the compressed cavity gas. In these simulations, the focal spot radius was fixed at $r_{foc}=0.4$ mm, while the pulse duration t_p was varied. The three cases shown in Fig. 3 have been realized by assigning the following target proportions: (a) solid Au sample: $R_0=r_{foc0}=0$, $R_{l0}=1.5r_{foc}$; (b) exploding Au pusher: $r_{foc0}=0$, $R_0=0.7r_{foc}$, $R_{l0}=1.5r_{foc}$; and (c) cold Au pusher: $R_0=0.55r_{foc}$, $r_{foc0}=0.6r_{foc}$, $R_{l0}=1.5r_{foc}$. The effect of pressure enhancement due to the hydrodynamic cumulation in the converging flow is demonstrated by comparing the cases (b) and (c) with the reference case (a).

First of all note that, if the cavity at $r<R_0$ were void and the imploding liner material obeyed the laws of ideal hydrodynamics, the pressure on the cylinder axis at the time of void closure would be infinite.[11] In reality, the central pressure peak is always finite because of the initial gas fill and dissipation processes in the converging flow. Intuitively, it is clear that in the limit of large convergence ratios, $C_r\gg1$, the peak pressure P_{max} must be insensitive to the properties and the initial state of the fill gas: it should be determined solely by the liner configuration, energy deposition in the liner, and the value of C_r. Here the radial convergence ratio C_r is defined for the gas/metal (D/Au) interface,

$$C_r=\frac{R(0)\equiv R_0}{R(t_{max})}, \tag{3}$$

where t_{max} is the time when the pressure at $r=0$ reaches its peak value P_{max}.

The main conclusion from Fig. 3 is that the pressure enhancement factor has modest values of 1.2–1.5 in the case of an exploding pusher, and becomes as high as 10 and larger in the case of a cold pusher. Our simulations indicate also that the peak pressure obtained with the exploding pusher is virtually independent of C_r when $C_r>10$; for a cold pusher, on the contrary, it increases noticeably with C_r. At this stage, it would be premature to fix any upper limit for realistic values of C_r in these types of implosions. Trying not to set unjustified limits, we assume tentatively that any value of $C_r\lesssim100$ might be feasible. When calculating the curves (b) and (c) in Fig. 3, the initial fill gas parameters ρ_0, T_0 were adjusted such as to keep the C_r values in the range $20\lesssim C_r\lesssim40$: (b) $\rho_0=3\times10^{-4}$ g/cm^3, $T_0=1$ eV, full bremsstrahlung and conduction losses; (c) $\rho_0=3\times10^{-4}$ g/cm^3, $T_0=5$ eV, adiabatic compression of the fill gas. With these parameters, the values of C_r varied between $C_r=30$ for $t_p=200$ ns and $C_r=40$ for $t_p=1$ ns in case (b), and between $C_r=24$ for $t_p=200$ ns and $C_r=42$ for $t_p=1$ ns in case (c).

In view of clear advantages offered by implosions with a cold pusher, we consider only this case in what follows. The geometric target proportions used in all subsequent simulations are those given for the case (c) above. As a precaution against the Rayleigh–Taylor instability at the pusher–absorber interface $r=r_{foc0}$, the initial aspect ratio of the cold pusher, $A_p=r_{foc0}/(r_{foc0}-R_0)=12$, is chosen to be not too high (for more details see Sec. IV D).

III. QUASIADIABATIC COMPRESSION OF THE CENTRAL GAS

Let us assume for the moment that the deuterium gas in the central cavity has uniform temperature and density distributions and implodes quasiadiabatically. Then, its parameters would scale as

$$\rho=\rho_0C_r^2,\quad \rho R=(\rho R)_0C_r,\quad T=T_0C_r^{4/3}, \tag{4}$$

with the radial convergence ratio C_r. Hence, with an initial preheat of $T_0\simeq20-30$ eV one could reach temperatures in the keV range and generate significant amounts of thermonuclear neutrons in quasiadiabatic implosions with $C_r\gtrsim30$. The main question addressed in this paper is under what conditions and how close can one approach this regime by using the effect of magnetothermal insulation.

The principal energy loss mechanisms from the fuel plasma under the conditions of interest are the bremsstrahlung radiation and the electron heat conduction. For a quasiadiabatic implosion, the ratio of the bremsstrahlung cooling time scale t_{ff} to the hydrodynamic time scale t_h,

$$\Gamma_{ff}\equiv\frac{t_{ff}}{t_h}=2.0\times10^{-9}\bar{A}\frac{UT_{keV}^{1/2}}{\rho R}\propto\frac{T_0^{1/2}}{(\rho R)_0}UC_r^{-1/3}, \tag{5}$$

scales only weakly with C_r. Hence, the bremsstrahlung cooling can be brought down by choosing a sufficiently low initial value of the fuel ρR. In Eq. (5), A is the mean atomic mass of the hydrogen-isotope plasma, $U=|dR/dt|$ is the implosion velocity, T_{keV} is the fuel temperature in keV; we use the CGS units in all the practical formulas. Specific details on definitions of t_{ff} and t_h are given in the Appendix.

The role of the heat conduction losses is characterized by the Péclet number,

$$\mathrm{Pe}\equiv\frac{t_{\mathrm{cc}}}{t_h}=\frac{n_e U R}{\kappa}, \tag{6}$$

where t_{cc} is the time scale for conduction cooling, κ is the heat conduction coefficient, n_e is the electron number density in a fully ionized plasma of hydrogen isotopes (for details see the Appendix). Clearly, in quasiadiabatic implosions we must have $\mathrm{Pe}\gg 1$. In the nonmagnetized case we can use the Spitzer conductivity, $\kappa=\kappa_e\propto T^{5/2}$, which yields the scaling

$$\mathrm{Pe}\propto\frac{(\rho R)_0}{T_0^{5/2}}UC_r^{-7/3}, \tag{7}$$

for quasiadiabatic implosions. This scaling tells us that, even when we start with $\mathrm{Pe}\gg 1$, the Péclet number decreases rapidly in the course of implosion, and, finally, when it drops below 1, the fuel begins to lose entropy at an ever increasing rate. Note also that, in contrast to the Γ_{ff} parameter, the Péclet number scales in direct proportion with the initial fuel ρR. The latter means that, trying to keep both the Γ_{ff} and the Pe values as large as possible, we will find (for a given T_0) an optimum for the parameter $(\rho R)_0$.

The above arguments are illustrated in Fig. 4 (see also Fig. 8) with three series of 1-D simulations of nonmagnetized implosions. In these simulations, the target dimensions (corresponding to $r_{\mathrm{foc}}=0.8\,\mathrm{mm}$), the ion pulse characteristics ($\epsilon=100$ kJ/g, $t_p=100\,\mathrm{ns}$), and the initial deuterium temperature $T_0=20\,\mathrm{eV}$ were kept fixed, while the initial deuterium density ρ_0 was varied between 3×10^{-5} and $10^{-3}\,\mathrm{g/cm^3}$. One clearly sees that, when both the bremsstrahlung and the conduction cooling are accounted for (black diamonds), the peak temperature does not rise above 180 eV, and the thermonuclear neutron yields remain relatively low. The optimum (for achieving a maximum peak temperature) value of the $(\rho R)_0$ parameter corresponds to $\rho_0\approx10^{-4}\,\mathrm{g/cm^3}$. Once, however, the heat conduction (both electronic and ionic) is fully suppressed ($\mathrm{Pe}=\infty$; black dots in Fig. 4), the results for low enough initial densities, $\rho_0\lesssim10^{-4}\,\mathrm{g/cm^3}$, become virtually indistinguishable from the pure adiabatic case [a thick gray line in Fig. 4(a)] and the peak deuterium temperature rises well above 1 keV. This gives us a hope that, by suppressing the radial heat conduction with a strong magnetic field, we can possibly reach keV temperatures and significant neutron yields in implosion experiments with a specific driver power deposition as low as $\dot{\epsilon}\simeq1$ TW/g. In the next section we analyze conditions required for such a regime of magnetically insulated implosions.

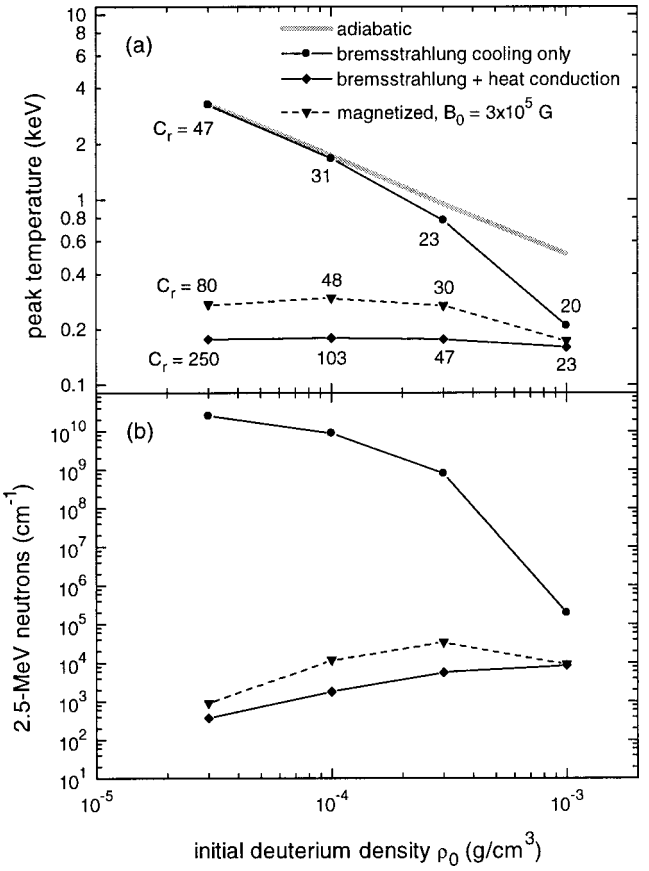

FIG. 4. Implosion results for $r_{\mathrm{foc}}=0.8\,\mathrm{mm}$, $t_p=100\,\mathrm{ns}$, $T_0=20\,\mathrm{eV}$, and four different values of ρ_0. Diamonds, dots and a thick gray line represent nonmagnetized ($B_0=0$) implosions under different assumptions about the cooling losses from the deuterium plasma. Magnetized implosions with $B_0=3\times10^5$ G are shown with triangles. (a) Peak values of the plasma temperature averaged over the central 10% of the deuterium mass. For each implosion the corresponding value of the radial convergence ratio C_r is indicated. (b) Total numbers of 2.5 MeV DD neutrons generated in the corresponding implosions.

IV. MAGNETIZED IMPLOSIONS

A. Self-sustained regime of magnetized implosion

Assume now that a transverse (with respect to the radial direction) magnetic field B is introduced into a cylindrical fuel plasma volume with parameters ρ, T, R. In principle, this could be either a z field or a ϕ field, or a combination of both. In this paper we consider only the case of a z field because the latter has an advantage of attaining its maximum on the cylinder axis (whereas the ϕ field must vanish there)—exactly where the temperature peaks and where the effects of magnetic insulation are mostly needed. Also, the z field is compressed more effectively ($B\propto C_r^2$) than the ϕ field ($B\propto C_r$) in cylindrical implosions of ideally conducting plasma columns.

The impact of a macroscopic magnetic field on the electron transport coefficients is characterized by the magnetization parameter,

$$x_e=\omega_e\tau_e=3.18\times10^{-7}A\frac{B}{\rho}\frac{T_{\mathrm{keV}}^{3/2}}{L_{ei}}, \tag{8}$$

where $\omega_e = eB/m_e c$ is the electron cyclotron frequency, τ_e is the electron–ion collision time,[12] and L_{ei} is the Coulomb logarithm; in all practical formulas, the field strength B is in Gauss. When we substitute the Braginskii formula[12] for the transverse electron heat conduction coefficient $\kappa = \kappa_{e\perp}$ into Eq. (6), we obtain the following expression for the Péclet number:

$$\mathrm{Pe} = 3.15\times 10^{-5} UR \frac{\rho L_{ei}}{A T_{\mathrm{keV}}^{5/2}} \frac{3.77 + 14.79 x_e^2 + x_e^4}{11.92 + 4.664 x_e^2}. \tag{9}$$

In the case of strong magnetization, when $x_e \gg 1$, the electron heat conduction is suppressed by a factor $\approx x_e^2$, and the Péclet number is increased correspondingly.

It should be noted here that in strongly magnetized plasmas with $x_e \gg 1$ the ion heat conduction becomes also important, and, strictly speaking, we should use the sum $\kappa = \kappa_{e\perp} + \kappa_{i\perp}$ in Eqs. (6) and (9). We ignore the ion conductivity when analyzing the qualitative aspects, scalings, and optimal initial conditions for magnetized implosions in this and the next sections, but it is fully accounted for in numerical simulations discussed in Sec. IV C.

In the ideal case we want to have a radial implosion with a fully frozen-in magnetic field, when the magnetic flux in each plasma element is conserved. The ability to preserve the magnetic flux is characterized by the magnetic Reynolds number,

$$\mathrm{Rm} \equiv \frac{t_{b\mathrm{dif}}}{t_{bh}} = \frac{2\pi}{c^2} \sigma_\perp UR, \tag{10}$$

where $t_{b\mathrm{dif}}$ is the time scale for radial diffusion of the magnetic field, t_{bh} is the time scale for ideal hydrodynamic compression of this field (for more details see the Appendix), $\sigma_\perp$ is the transverse plasma conductivity, and c is the speed of light. Evidently, we need $\mathrm{Rm} \gg 1$ for effective compression of the frozen-in magnetic field.

In general, we have to distinguish between two different magnetic Reynolds numbers for the target configuration shown in Fig. 1: one for the pusher, Rm_p, and the other for the deuterium gas, Rm_f. A separate value of Rm_p is needed for the cold metallic pusher because its initial conductivity is typically one to three orders of magnitude higher than that of the fuel plasma preheated to $T_0 \simeq 10-30$ eV. In the course of implosion, however, the value of Rm_p decreases (because the conductivity $\sigma_{p\perp}$ of a metallic pusher decreases as it heats up, and because the radius R becomes smaller), while the value of Rm_f typically increases (because the fuel conductivity, $\sigma_{f\perp} \propto T^{3/2}$, grows with temperature). Hence, even when the magnetic field is initially confined by a highly conducting cold pusher ($\mathrm{Rm}_p \gg 1$), one still has to ensure $\mathrm{Rm}_f \gg 1$ at later stages of implosion if thermonuclear plasma parameters are to be reached. To simplify the qualitative and scaling analysis, we consider in the first place the Rm number of the fuel,

$$\mathrm{Rm} = \mathrm{Rm}_f = \frac{2\pi}{c^2} \sigma_{f\perp} UR = 0.019 UR \frac{T_{\mathrm{keV}}^{3/2}}{L_{ei}}, \tag{11}$$

but remember that a high initial value of Rm_p allows us to reduce the initial threshold for Rm_f to $\simeq 0.3-1$. In Eq. (11), $\sigma_{f\perp} = e^2 n_e \tau_e / m_e$ is the transverse conductivity of a strongly magnetized hydrogen plasma (for $B=0$ this conductivity becomes a factor 1.96 higher).[12]

Thus, the quality of magnetic insulation of the imploding fuel is controlled by the values of three dimensionless parameters x_e, Pe, and Rm: once the values $x_e \gg 1$, $\mathrm{Pe} \gg 1$, $\mathrm{Rm} \gg 1$ are established, the fuel plasma is compressed quasiadiabatically (provided that the radiation cooling is unimportant) with a frozen-in magnetic field. In this case, under the assumption of uniform radial profiles, the above three parameters scale as

$$x_e \propto C_r^2, \quad \mathrm{Pe} \propto U C_r^{5/3}, \quad \mathrm{Rm} \propto U C_r, \tag{12}$$

with the radial convergence ratio C_r, and all three only continue to grow in the course of implosion with a given implosion velocity U. As a result, we obtain a self-sustained regime of magnetized implosion, whose quality in confining the entropy and magnetic flux only improves as the flow converges toward the axis. One can verify that the SSMI regime is parametrically unstable in the sense that, once the values of either Pe or Rm fall below unity, the imploding fuel begins to loose entropy and magnetic flux at an ever increasing rate, and the implosion deviates only further away from the magnetically insulated regime.

B. Initial conditions for the SSMI regime

Here we examine plasma parameters required for initiating the self-sustained regime of magnetized implosion. First of all note that the SSMI regime should not start necessarily with $x_e > 1$. If we have initially $x_e \ll 1$ combined with $\mathrm{Pe} \gg 1$ and $\mathrm{Rm} \gg 1$, the implosion still proceeds in the quasiadiabatic mode with a frozen-in magnetic field until the decreasing Péclet number, $\mathrm{Pe} \propto U C_r^{-7/3}$, drops below unity. If, however, the magnetization parameter—which grows as $x_e \propto C_r^2$—becomes larger than unity before this happens, such an implosion enters the SSMI regime as well. One readily verifies that both situations (with $x_e < 1$ and $x_e > 1$) can be accounted for by setting a lower limit on the initial value of the product,

$$x_e \,\mathrm{Pe}_1 = 1.18\times 10^{-11} \frac{URB}{T_{\mathrm{keV}}}, \tag{13}$$

where Pe_1 is the value of the Péclet number in Eq. (9) at $x_e = 1$. Note that the product $x_e \,\mathrm{Pe}_1$ scales only weakly, $x_e \,\mathrm{Pe}_1 \propto U C_r^{-1/3}$, with the convergence ratio C_r in quasiadiabatic implosions.

Finally, we conclude that a plasma column with initial parameters ρ_0, T_0, R_0, and B_0 can enter the SSMI regime with an implosion velocity U only when the conditions

$$x_e \,\mathrm{Pe}_1 = 1.18\times 10^{-11} \frac{UR_0 B_0}{T_{0,\mathrm{keV}}} \geqslant \mathcal{P}e_0, \tag{14}$$

$$\mathrm{Rm} = 0.019 \frac{UR_0 T_{0,\mathrm{keV}}^{3/2}}{L_{ei}} \geqslant \mathcal{R}m_0, \tag{15}$$

are satisfied; here $\mathcal{P}e_0$ and $\mathcal{R}m_0$ are certain numbers on the order of, or greater than 1. Inequalities (14) and (15) imply that, for a given initial magnetic field B_0, there is an optimum value of the initial fuel temperature,

$$T_{0,\mathrm{opt}}=20\ \mathrm{eV}\left(\frac{B_0}{10^5\ \mathrm{G}}\right)^{2/5}\left(\frac{\mathcal{R}m_0L_{ei}}{\mathcal{P}e_0}\right)^{2/5}, \tag{16}$$

and an ''absolute'' (independent of T_0, ρ_0, R_0) lower bound on the product UR_0,

$$UR_0\geqslant 1.8\times 10^4\frac{\mathrm{cm}^2}{\mathrm{s}}\left(\frac{10^5\,\mathrm{G}}{B_0}\right)^{3/5}\mathcal{P}e_0^{3/5}(\mathcal{R}m_0L_{ei})^{2/5}, \tag{17}$$

required for the regime of self-sustained magnetized implosion. Note that the initial plasma density ρ_0 does not enter Eqs. (14)–(17). This means that, once the fuel is preheated to the optimum temperature (16) and the condition (17) is fulfilled, the value of ρ_0 can be used to bring under control the bremsstrahlung energy losses.

The above arguments can be easily repeated for a less interesting case of low-temperature magnetized implosions, characterized by a negligible role of the fuel plasma conductivity $\sigma_{f\perp}$ compared to the pusher conductivity $\sigma_{p\perp}$. In this case one also obtains an ''absolute'' lower limit on the product UR_0 from the condition $\mathrm{Rm}=\mathrm{Rm}_p\geqslant\mathcal{R}m_0$ but no constraint from below on the initial fuel temperature T_0.

C. 1-D MHD simulations of magnetized cylindrical implosions

In order to reach the SSMI regime in implosions driven by ion beams, one has in the first place to satisfy the criterion (17). For a fixed specific energy deposition of $\epsilon=100$ kJ/g we have more or less fixed implosion velocity $U\approx 10^6$ cm/s, provided that the ion pulse duration t_p does not exceed the implosion time $t_{\mathrm{im}}=R_0/U$. Then, for $\mathcal{P}e_0\approx 3$, $\mathcal{R}m_0\approx 1$, $L_{ei}\approx 7$, Eq. (17) implies a lower limit of

$$R_0\gtrsim 0.8\ \mathrm{mm}\left(\frac{10^5\ \mathrm{G}}{B_0}\right)^{3/5}, \tag{18}$$

on the initial fuel cavity radius and, consequently, on the focal spot radius of the ion beam. In other words, a critical parameter for achieving the SSMI regime is not the intensity of the ion irradiation but rather an extensive quantity associated with the mere energy scale of the experiment. More precisely, for a family of similar target configurations with proportions of the case (c) in Sec. II, the lower limit (17) on the product $UR_0\propto\epsilon^{1/2}r_{\mathrm{foc}}$ translates into the following constraint on the ion beam parameters:

$$\frac{N_i}{\rho}\left|\frac{dE_i}{dz}\right|\geqslant 0.34\frac{\mathrm{kJ}}{\mathrm{g/cm}^2}\left(\frac{10^5\ \mathrm{G}}{B_0}\right)^{6/5}\mathcal{P}e_0^{6/5}(\mathcal{R}m_0L_{ei})^{4/5}. \tag{19}$$

This criterion, applied with $\mathcal{P}e_0=3$, $\mathcal{R}m_0=1$, $L_{ei}=7$, tells us that the effects of magnetic insulation could marginally be demonstrated with the future TWAC beam ($\epsilon\approx 100$ kJ/g, $r_{\mathrm{foc}}\approx 0.8$–$1$ mm, $R_0\approx 0.4$–0.6 mm) if the initial field $B_0\approx 3\times 10^5$ G were provided. By contrast, in the 20 kJ option of the future HAR GSI beam, which should generate practically the same energy deposition of $\epsilon\approx 100$ kJ/g, but within a factor 2–2.5 smaller spot size, the total number of ions is too small to observe the advantages of magnetized implosions with feasible values of the initial field strength B_0. This conclusion is also confirmed by the detailed 1-D MHD simulations.

For the MHD simulations, the target configuration was set exactly as it is described in Sec. II. The implosion is driven by uniform heating of the gold liner in the annular region $r_{\mathrm{foc}0}<r<r_{\mathrm{foc}}$ with a fixed total specific energy deposition of $\epsilon=100$ kJ/g. The focal radius r_{foc}, the ion pulse duration t_p, the initial deuterium gas parameters ρ_0, T_0, and the strength B_0 of the initially uniform axial magnetic field are treated as free parameters. Simulations have been performed with the upgraded version of the 1-D three-temperature Lagrangian hydrodynamics code DEIRA.[13] In its MHD version, the DEIRA code solves a 1-D system of single-fluid dissipative magnetohydrodynamics equations deduced from the Braginskii two-fluid equations[12] for the particular case of cylindrical (or planar) geometry with a purely axial magnetic field; the terms with the electron viscosity are omitted. The effects of the magnetic field on all the transport coefficients—including the electron and ion heat conductivities, electrical conductivity, ion viscosity, and alpha particle diffusion—are properly accounted for by using the formulas from Refs. 12 and 14.

Three series of MHD simulations have been performed for three different values of the focal radius r_{foc}, namely $r_{\mathrm{foc}}=0.4$ mm (with $t_p=50$ ns), $r_{\mathrm{foc}}=0.8$ mm (with $t_p=100$ ns), and $r_{\mathrm{foc}}=4$ mm (with $t_p=100$ ns). The results for the first case of $r_{\mathrm{foc}}=0.4$ mm are not shown here because they are essentially negative: with $B_0\leqslant 5\times 10^5$ G the effects of target magnetization manifest themselves neither in the peak fuel temperature nor in the total neutron yield (note that for $r_{\mathrm{foc}}=0.4$ mm we have $R_0=0.22$ mm). The physical reason, expressed by conditions (18) and (19), is simply that the target size in this case is too small (for the given value of ϵ), and one cannot find a region in the parameter space with both $\mathrm{Pe}\gg 1$ and $\mathrm{Rm}>1$. As a result, either the heat or the magnetic field dissipate from the fuel volume faster than the latter collapses onto the axis.

The results obtained for $r_{\mathrm{foc}}=0.8$ mm are shown in Figs. 4–7. This case corresponds roughly to the parameters of the TWAC beam[1] and, according to Eqs. (18) and (19), is close to the threshold for the SSMI regime at $B_0\gtrsim 3\times 10^5$ G. Figure 4(a) demonstrates indeed that the peak plasma temperatures (the electron and ion temperatures are practically equal in all the cases considered) reached in magnetized implosions (triangles) exceed noticeably (by about a factor 1.7) those obtained without a magnetic field (diamonds), although they still remain well below the 1–3 keV range reached in simulations with the zero heat conduction (circles). Note that, in order to smooth out possible spurious numerical effects, Fig. 4(a) displays temperature values averaged over the inner 10% of the fuel mass, which typically contained eight mesh zones. The initial deuterium temperature in all the numerical runs was fixed at $T_0=20$ eV, which is close to the optimum value given by Eq. (16).

Figures 5, 6, and 7 display the dynamics of one implosion, namely the one starting at $\rho_0=10^{-4}$ g/cm^3, from the series plotted in Fig. 4. General hydrodynamical features

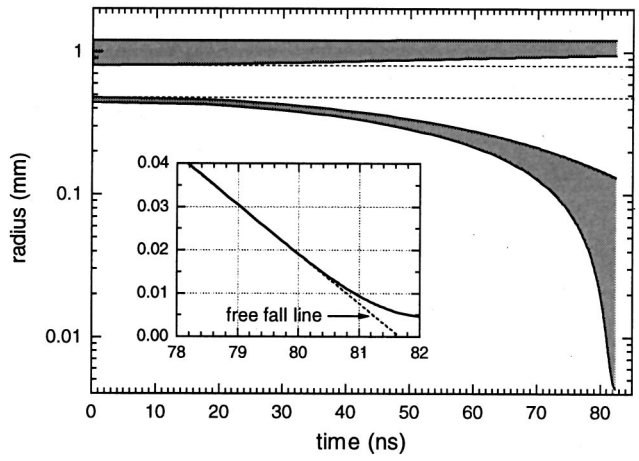

FIG. 5. Radius–time diagram of the magnetized implosion starting at $\rho_0 = 10^{-4}$ g/cm^3 from the series shown in Fig. 4. Plotted are the trajectories of the four Lagrangian elements initially at $r = R_0$, r_{foc0}, $r_{foc,}$ and R_{l0} as shown in Fig. 1. The beam heated region is the unshaded band between the two horizontal dashed lines. The lower shaded area corresponds to the cold pusher. The insert is a blowup of the pusher–fuel interface trajectory near the time of stagnation. The point $T_{max} = 295$ eV, $C_r = 48$ given in Fig. 4(a) is achieved at $t = 81.0$ ns.

shown in Figs. 5 and 6 are typical of all the implosions discussed in this paper. The inner boundary of the cold pusher, initially at $r = R_0$, accelerates at an approximately constant rate to a maximum implosion velocity of $U \approx 1.1 \times 10^6$ cm/s. The cold pusher behaves itself almost as incompressible fluid: most of the time its temperature and density are stabilized at a level of $T \approx 2000$ K, $\rho \approx 20$ g/cm^3; its in-flight aspect ratio (IFAR) steadily decreases in the course of implosion (note that a constant IFAR would correspond to a constant vertical size of the pusher area in Fig. 5 along the logarithmic scale for the radius). The deuterium temperature peaks at $t = 81.0$ ns when its radius converges by a factor of $C_r = 48$. The pressure and density profiles in Fig. 6 are given for the time $t = 81$ ns of the temperature peak, for $t = 80$ ns at half the radial convergence of the temperature peak, and for $t = 50$ ns when the pusher is accelerated to about one-half its peak implosion velocity.

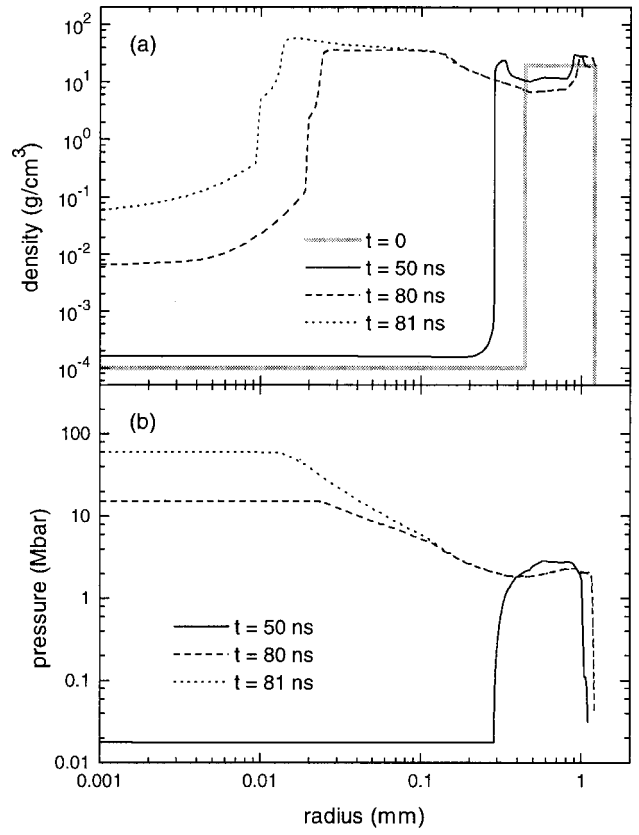

FIG. 6. Density (a) and pressure (b) profiles at three characteristic times in the same implosion as in Fig. 5.

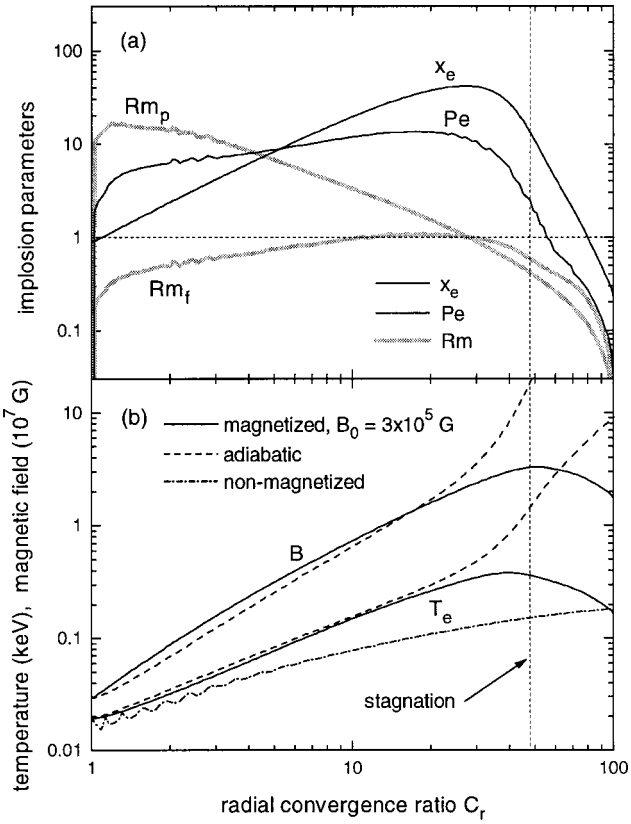

FIG. 7. (a) Evolution of the principal dimensionless parameters in the same implosion as shown in Figs. 5 and 6. The value $C_r = 48$, corresponding to the temperature peak in Fig. 4(a), is marked as a stagnation point. (b) Evolution of the central values of the magnetic field strength B and the electron temperature T_e in the same magnetized implosion (solid curves) compared with the fully frozen in, $B = B_0(\rho/\rho_0)$, and the adiabatic, $T = T_0(\rho/\rho_0)^{2/3}$, laws (dashed curves). The dashed–dotted curve shows the central temperature in the corresponding nonmagnetized ($B_0 = 0$) implosion with the same value of ρ_0 and full (bremsstrahlung+heat conduction) energy losses.

Evolution of the main parameters that characterize the fuel magnetization is shown in Fig. 7. Here physical quantities are plotted versus current value $C_r = C_r(t) = R_0/R(t)$ of the radial convergence ratio. It is clearly seen that up to the moment of $C_r = 25$–30 the plasma parameters evolve qualitatively, as predicted for the SSMI regime. A somewhat weaker scaling of x_e, Pe, and Rm_f with C_r than predicted by Eq. (12) is due to the increasing nonuniformity of the radial temperature and density distributions (see Fig. 10 below). Once, however, both the Rm_p and Rm_f magnetic Reynolds numbers drop below unity at $C_r \approx 30$, the fuel volume begins

to lose rapidly the magnetic flux and the entropy, which is reflected in turning down of the x_e and Pe curves. Figure 7(b) shows also that both the magnetic field and the electron temperature on the target axis follow closely the ideal magnetized laws as long as $\mathrm{Rm}_p > 1$ and $\mathrm{Rm}_f > 1$, i.e., up to $C_r \approx 30$.

Two different magnetic Reynolds numbers plotted in Fig. 7(a) illustrate different roles of the pusher and fuel conductivities in confining the magnetic field: for Rm_p we use the maximum conductivity value $\sigma_{p\perp}$ in the cold pusher layer, and Rm_f is calculated by using the deuterium plasma conductivity $\sigma_{f\perp}$ at $r=0$. One clearly sees that the dominant role in compressing the magnetic field and supporting the SSMI regime belongs to a relatively high conductivity of the pusher. We are inevitably led to this regime when we want to obtain a magnetized implosion with a relatively low implosion velocity U and the smallest possible radial size R_0. Under such conditions, the imploding pusher is typically in a state of a liquid metal whose conductivity $\sigma_{p\perp}$ is inversely proportional to the temperature. Hence, it is important to keep the entropy of the imploding pusher as low as possible.

The enhancement of the total 2.5 MeV neutron yield due to the target magnetization [triangles versus diamonds in Fig. 4(b)] is below factor 10 and appears as rather modest. This is partly because most of the neutrons in the nonmagnetized case are generated at rather high values of the convergence ratio $C_r \gtrsim 100$, which are not reached in the magnetized case and may be unattainable in real experiments. The realistic situation for the neutron diagnostics may, in fact, be more favorable than it is implied by Fig. 4(b). This is suggested by the following result: if we evaluate the total numbers of neutrons generated in the magnetized and nonmagnetized cases up to a fixed value of $C_r = 30$, the difference between the two cases turns out to be almost a factor 1000.

To illustrate the properties of magnetized implosions in the case when condition (17) is fulfilled with a significant margin, we have simulated also a larger target with $r_{\mathrm{foc}} = 4.0\,\mathrm{mm}$. The results obtained for $T_0 = 20\,\mathrm{eV}$, $B_0 = 10^5\,\mathrm{G}$ are shown in Figs. 8 and 9, which are analogous to Figs. 4 and 7. Now the peak temperature in magnetized implosions exceeds by a factor 4–5 the nonmagnetized values [see Fig. 8(a)], and temperature values above 1 keV are reached for $\rho_0 \lesssim 3\times10^{-5}\,\mathrm{g/cm^3}$. The main plasma parameters, plotted in Fig. 9 for the case of $\rho_0 = 3\times10^{-5}\,\mathrm{g/cm^3}$, evolve, as expected in the SSMI regime. The behavior of the Rm_p and Rm_f curves in Fig. 9(a) tells us that initially, at $C_r \lesssim 10$, the magnetic field is confined by the conductivity of the metallic pusher, whereas at a later stage, beyond $C_r \gtrsim 20$, the conductivity of the hydrogen plasma becomes more important.

The increase in the neutron production due to the target magnetization, shown in Fig. 8(b), is much less dramatic than one would expect from the temperature increase displayed in Fig. 8(a). The cause is that, by the time of stagnation, the hot magnetized fuel core comprises only about 10% of the total fuel mass. Figure 10 shows that most of the fuel mass—which is initially uniformly preheated to $T_0 = 20\,\mathrm{eV}$—has been snowplowed into a thin dense boundary layer between the cold pusher and the hot central spot.

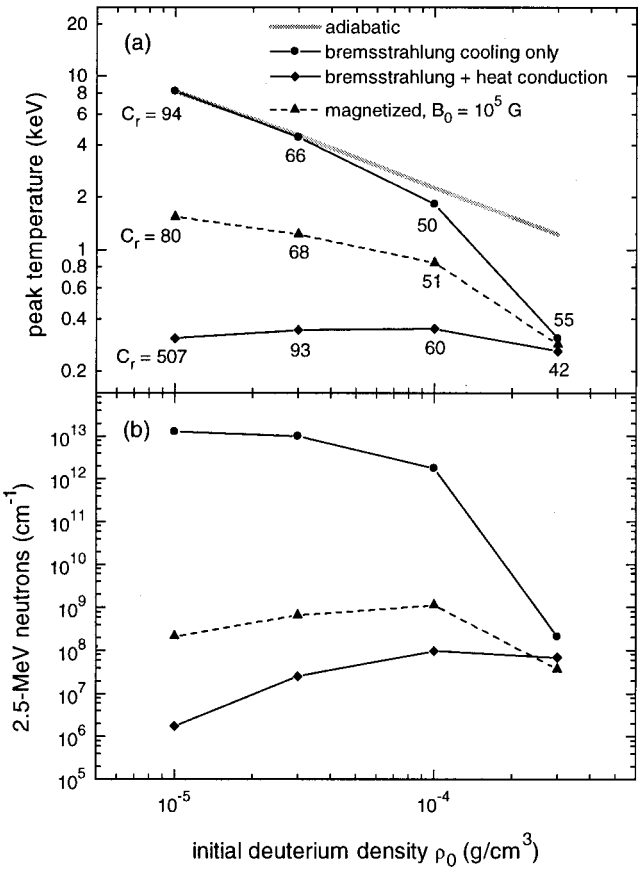

FIG. 8. The same as Fig. 4 but for $r_{\mathrm{foc}} = 4.0\,\mathrm{mm}$, $B_0 = 10^5\,\mathrm{G}$.

This strong departure from the uniform compression explains also why the x_e, Pe, and Rm_f parameters in Fig. 9(a) scale weaker with C_r than predicted by Eq. (12).

As a remark on the dynamic role of the magnetic pressure, we note that in our case the **j×B** force manifests itself as a gradient of the magnetic pressure $P_m = B^2/8\pi$. For implosions considered here, the magnetic pressure P_m is already initially at least comparable to the plasma pressure P_g in the fuel region. They both, however, have little effect on the implosion dynamics until the stagnation phase is approached. At stagnation, the magnetic pressure—which scales as $P_m \propto \rho^2$ compared to $P_g \propto \rho^{5/3}$ for the plasma pressure—typically strongly dominates in the hot magnetized core, while P_g prevails at the cold fuel periphery (see Fig. 10). In other words, the pusher implosion is finally halted by the magnetic pressure in the hot fuel core. This should be a typical situation for implosions optimized for maximum magnetization effects because for smaller initial fields B_0 the magnetic insulation effects become weaker, while for still larger B_0 the magnetic pressure becomes too high and halts the implosion too early before high enough values of C_r are reached. For the case presented in Figs. 9 and 10, the initial field $B_0 = 10^5\,\mathrm{G}$ corresponds just to such an optimum between the two extreme cases.

D. On the role of hydrodynamic instabilities

An important issue for the implosions considered here is the hydrodynamic stability of the cold pusher layer. The

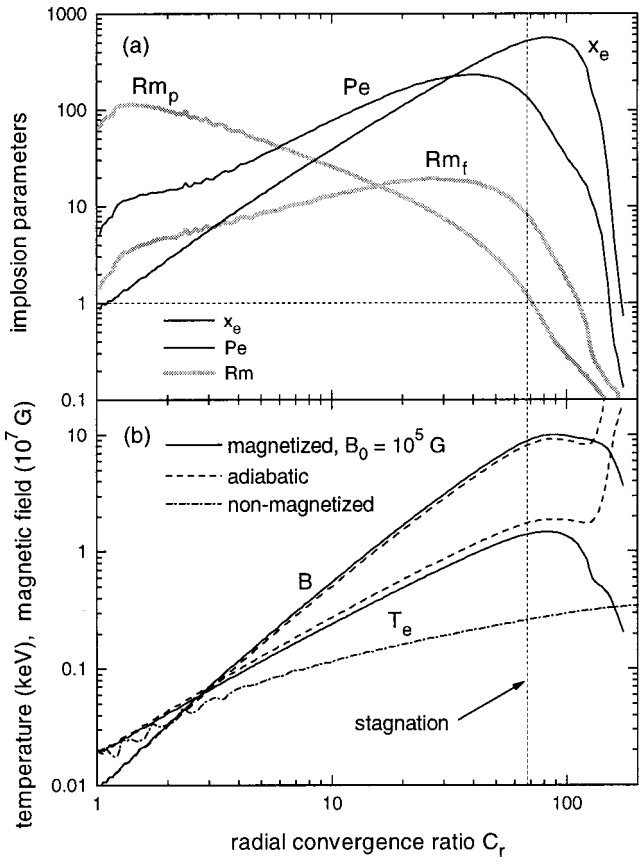

FIG. 9. The same as Fig. 7 but for $r_{foc}=4.0$ mm, $B_0=10^5$ G, $\rho_0=3\times10^{-5}$ g/cm^3.

outer pusher boundary (initially at $r=r_{foc0}$) becomes Rayleigh–Taylor unstable during the acceleration stage, which is seen from the pressure and density profiles for $t=50$ ns in Fig. 6. It is a known fact that when a heavy shell of incompressible fluid is accelerated by a light gas [high-density contrast, the Atwood number $\mathrm{At}=(\rho_1-\rho_2)/(\rho_1+\rho_2)\approx1$], it travels some seven to ten of its own thicknesses before being ruptured by the instability.[15] In our case the growth of this instability is mitigated (i) by the zero initial value of the Atwood number (no initial density contrast), and (ii) by the finite density gradient that develops between the heated absorber layer and the cold pusher. Since the pusher IFAR only decreases with time, we can expect that a pusher with an initial aspect ratio around 10 should survive the Rayleigh–Taylor instability of the acceleration stage. A detailed investigation of this issue remains, however, for future work.

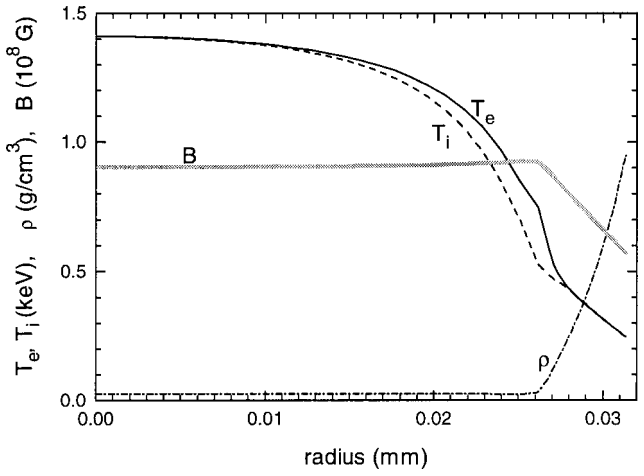

FIG. 10. Radial temperature, density, and magnetic field profiles in the deuterium region at the time of stagnation in the implosion shown in Fig. 9. The hot magnetized core at $r<0.026$ mm contains about 10% of the total deuterium mass.

The inner pusher boundary (initially at $r=R_0$) becomes unstable during the deceleration stage near the stagnation time (see the density and pressure profiles for $t=80$ and 81 ns in Fig. 6). Here the so-called freefall line of the pusher–fuel interface (see the insert in Fig. 5) gives an indication of how deep the ''fingers'' of the heavy pusher material can penetrate into the fuel. In Fig. 5 it is seen that, by the time the temperature peaks at $t=81.0$ ns, the deviation of the free-fall line from the 1-D pusher boundary trajectory does not exceed 20%. From this we conclude that the 1-D peak fuel parameters calculated in this paper should not be strongly affected by the pusher–fuel mixing at the deceleration stage. More restrictive constraints can be expected from the non-uniformities of the beam irradiation and fabrication errors. Note also that the pusher–fuel mixing may be much more of an issue in ignition MTF targets because, as it is shown in Fig. 10, most of the fuel mass may be finally scooped into a thin cold layer near the pusher boundary.

V. CONCLUSION

Ion beams planned to be available in the near future at GSI (Darmstadt) and ITEP (Moscow) will be capable of delivering up to $\simeq$100 kJ/g of energy deposition on target on a time scale of 50–100 ns. The beam irradiation geometry is well suited for conducting cylindrical implosion experiments. In the implosion scheme with a cold heavy pusher, the initial pressure created by the beam heating can be enhanced by more than a factor of 10 due to radial convergence of the hydrodynamic flow. As a result, pressure values in excess of 100 Mbar can be reached in the compressed target core along the cylinder axis. This should open interesting new possibilities for investigating properties of matter at high energy densities.

A new dimension to these types of experiments could be added by the introduction of a magnetic field. The magnetic field suppresses heat conduction losses in the radial direction and allows us to enhance considerably the peak temperature values that can be reached in deuterium (or deuterium–tritium) plasma columns compressed by an imploding liner. Parametric analysis of magnetized implosions shows that the advantages of magnetothermal insulation can be fully exploited only when a regime of self-sustained magnetized implosion is reached. It is demonstrated how simultaneous constraints on the magnetic Reynolds and the Péclet numbers lead to a lower limit (17) on the product UR of the implosion velocity U by the plasma radius R as the principal condition for reaching the SSMI regime. Derived for a cylinder, this condition applies—apart from different numerical

factors—to spherical and planar implosions as well. A notable feature of the SSMI regime is that the quality of the magnetothermal insulation only improves in the course of implosion once the regime sets in, and deteriorates otherwise.

If magnetized cylindrical implosions are driven by fast ion beams, the threshold for the SSMI regime is determined by the total driver energy investment per unit areal density of the cylinder, $\rho^{-1}|dE_b/dz|$. The 1-D MHD simulations demonstrate that the advantages of magnetized implosions can already be observed at specific energy and power deposition levels as low as $\epsilon \simeq 100$ kJ/g and $\dot{\epsilon} \simeq 1$ TW/g, provided that the total number of ions in the beam N_i is sufficiently large. The marginal case corresponds roughly to the TWAC beam parameters.[1] For still larger N_i values, keV temperatures and significant neutron yields can be achieved in magnetized implosions of preheated deuterium plasma cylinders.

The results presented in this paper have been obtained in the framework of a 1-D model, with the main goal to elucidate general properties of magnetized implosions and to point out a possible direction for future experiments with intense ion beams. In reality, drive asymmetries, target imperfections and instabilities near the stagnation state will distort to a certain extent our 1-D results and lead to additional restrictions on peak plasma parameters. The analysis of these aspects, however, should refer to a more accurately specified experimental conditions and remains for the future work.

ACKNOWLEDGMENTS

This work was performed during a four-month stay at the Gesellschaft für Schwerionenforschung (Darmstadt). The author is grateful to Professor D. H. H. Hoffmann and all members of his group for hospitality, support, and stimulating discussion. Very useful and stimulating also, have been discussions with M. D. Churazov, A. A. Golubev, I. Hofmann, A. Kemp, B. Yu. Sharkov, and P. Spiller.

APPENDIX: DEFINITIONS OF THE RELEVANT TIME SCALES

To define the necessary time scales with specific values of the numerical coefficients, we make use of the following simple model for an imploding cylindrical plasma column. For the heating and cooling processes, we assume the simplest physically relevant temperature and velocity profiles,

$$T(t,r) = T_c(t)[1-(r/R)^2], \tag{A1}$$

$$u(t,r) = -rU/R, \tag{A2}$$

where $R(t)$ and $U(t) = -dR/dt$ are functions of t only. By substituting these profiles into the hydrodynamic energy equation,

$$\frac{\partial \epsilon}{\partial t} + u\frac{\partial \epsilon}{\partial r} + \frac{P}{\rho r}\frac{\partial}{\partial r}(ru) = -\frac{Q_{ff}}{\rho} + \frac{1}{\rho r}\frac{\partial}{\partial r}\left(r\kappa\frac{\partial T}{\partial r}\right), \tag{A3}$$

setting $r=0$ and using the ideal-gas equation of state for the hydrogen isotope plasma,

$$\epsilon = 3n_eT/\rho, \quad P = 2n_eT, \tag{A4}$$

we obtain the following equation for the temporal evolution of the central temperature $T_c(t)$:

$$\frac{dT_c}{dt} = \frac{4}{3}T_c\frac{U}{R} - \frac{Q_{ff}(n_e,T_c)}{3n_e} - \frac{4}{3}\frac{\kappa T_c}{n_eR^2}. \tag{A5}$$

Here

$$Q_{ff}(n_e,T) = 5.36\times10^{-24}n_e^2T_{\mathrm{keV}}^{1/2} \quad (\mathrm{erg\,cm^{-3}\,s^{-1}}) \tag{A6}$$

is the bremsstralung cooling rate per unit volume. The three terms on the right-hand side of Eq. (A5) represent, respectively, the rates of the adiabatic heating, bremsstrahlung cooling, and heat conduction cooling in the central region of an imploding cylindrical volume. Each of these terms implies a corresponding time scale:

$$t_h = \frac{3}{4}\frac{R}{U}, \quad t_{ff} = \frac{3n_eT}{Q_{ff}}, \quad t_{\mathrm{cc}} = \frac{3}{4}\frac{n_eR^2}{\kappa}. \tag{A7}$$

The ratio between thus defined time scales t_{ff} and t_h yields parameter Γ_{ff} in Eq. (5), and the ratio between t_{cc} and t_h leads to the definition (6) of the Péclet number Pe.

In the framework of the 1-D magnetohydrodynamics in cylindrical geometry with only an axial field component B, the evolution of $B=B(t,r)$ is governed by a single diffusion equation:

$$\frac{\partial B}{\partial t} + \frac{1}{r}\frac{\partial}{\partial r}(ruB) = \frac{c^2}{4\pi}\frac{1}{r}\frac{\partial}{\partial r}\left(\frac{r}{\sigma_\perp}\frac{\partial B}{\partial r}\right). \tag{A8}$$

By substituting the field profile,

$$B(t,r) = B_c(t)[1-(r/R)^2], \tag{A9}$$

together with the velocity profile (A2) into Eq. (A8) and setting $r=0$, we obtain the following equation for the temporal evolution of the central field value $B_c(t)$:

$$\frac{dB_c}{dt} = 2B_c\frac{U}{R} - \frac{c^2}{\pi}\frac{B_c}{\sigma_\perp R^2}. \tag{A10}$$

From this equation we calculate the values

$$t_{bh} = \frac{1}{2}\frac{R}{U}, \quad t_{b\mathrm{dif}} = \frac{\pi}{c^2}\sigma_\perp R^2, \tag{A11}$$

of the hydrodynamic, t_{bh}, and the diffusive, $t_{b\mathrm{dif}}$, time scales of the magnetic field evolution. The ratio between $t_{b\mathrm{dif}}$ and t_{bh} yields the definition (10) of the magnetic Reynolds number Rm.

[1] B. Yu. Sharkov, D. G. Koshkarev, M. D. Churazov, N. N. Alexeev, M. M. Basko, A. A. Golubev, and P. R. Zenkevich, Nucl. Instrum. Methods Phys. Res. A **415**, 20 (1998).
[2] N. Angert, Nucl. Instrum. Methods Phys. Res. A **415**, 236 (1998).
[3] I. Hofmann, ''Heavy ion inertial fusion in Europe,'' paper presented at the *13th International Symposium on Heavy Ion Inertial Fusion*, 13–17 March, 2000, San Diego; to appear in the special issue Nucl. Instrum. Methods, Phys. Res. A.
[4] N. A. Tahir, D. H. H. Hoffmann, J. A. Maruhn, K.-J. Lutz, and R. Bock, Phys. Plasmas **5**, 4426 (1998).
[5] N. A. Tahir, D. H. H. Hoffmann, A. Kozyreva, A. Shutov, J. A. Maruhn, U. Neuner, A. Tauschwitz, P. Spiller, and R. Bock, Phys. Rev. E **61**, 1975 (2000).
[6] F. S. Felber, M. A. Liberman, and A. L. Velikovich, Appl. Phys. Lett. **46**, 1042 (1985).
[7] F. S. Felber, M. M. Malley, F. J. Wessel, M. K. Matzen, M. A. Palmer, R.

B. Spielman, M. A. Liberman, and A. L. Velikovich, Phys. Fluids **31**, 2053 (1988).
[8]M. A. Liberman and A. L. Velikovich, J. Plasma Phys. **31**, 381 (1984).
[9]R. C. Kirkpatrick, I. R. Lindemuth, and M. S. Ward, Fusion Technol. **27**, 201 (1995).
[10]M. M. Basko, Sov. J. Plasma Phys. **10**, 689 (1984).
[11]Ya. B. Zel'dovich and Yu. P. Raiser, *Physics of Shock Waves and High-Temperature Hydrodynamic Phenomena* (Academic, New York, 1967), Vol. II, Chap. XII, Secs. 9,10.
[12]S. I. Braginskii, in *Reviews of Plasma Physics*, edited by M. A. Leontovich (Consultants Bureau, New York, 1965), Vol. 1, p. 205.
[13]M. M. Basko, Nucl. Fusion **30**, 2443 (1990).
[14]M. A. Liberman and A. L. Velikovich, J. Plasma Phys. **31**, 369 (1984).
[15]H. J. Kull, Phys. Rep. **206**, 199 (1991).